ACS OMEGA

Open Access

http://pubs.acs.org/journal/acsodf

Article

Facile and Bioinspired Approach from Gallic Acid for the Synthesis of Biobased Flame Retardant Coatings of Basalt Fibers

Alessia Pantaleoni,* Fabrizio Sarasini, Pietro Russo, Jessica Passaro, Loris Giorgini, Irene Bavasso, Maria Laura Santarelli, Elisabetta Petrucci, Federica Valentini, Maria Paola Bracciale, and Assunta Marrocchi

Cite This: *ACS Omega* 2024, 9, 19099−19107

Read Online

ACCESS | Metrics & More | Article Recommendations | Supporting Information

ABSTRACT: A sustainable, bioinspired approach to functionalize basalt fibers with an innovative gallic acid (GA)-iron phenyl phosphonate complex (BF-GA-FeP), for the purpose of improving the flame retardancy in composite materials, is developed. BFs were at first pretreated with O_3, obtaining surface free hydroxyl groups that allowed the subsequent covalent immobilization of biosourced GA units on the fiber through ester linkages. Phenolic −OH groups of the GA units were then exploited for the complexation of iron phenyl phosphonate, resulting in the target-complex-coated BF fiber (BF-GA-FeP). Microwave plasma atomic emission spectroscopy and scanning electron microscopy coupled with energy-dispersive X-ray spectroscopy analyses of BF-GA-FeP highlighted an increase in iron content, modification of fiber morphology, and occurrence of phosphorus, respectively. BFs, modified with a low amount of the developed complex, were used to reinforce a poly(lactic acid) (PLA) matrix in the production of a biocomposite (PLA/BF-FeP). PLA/BF-FeP showed a higher thermal stability than neat PLA and PLA reinforced with untreated BFs (PLA/BF), as confirmed by thermogravimetric analysis. The cone calorimeter test highlighted several advantages for PLA/BF-FeP, including a prolonged time to ignition, a reduced time to flame out, an 8% decrease in the peak heat release rate, and a 15% reduced fire propagating index compared to PLA/BF.

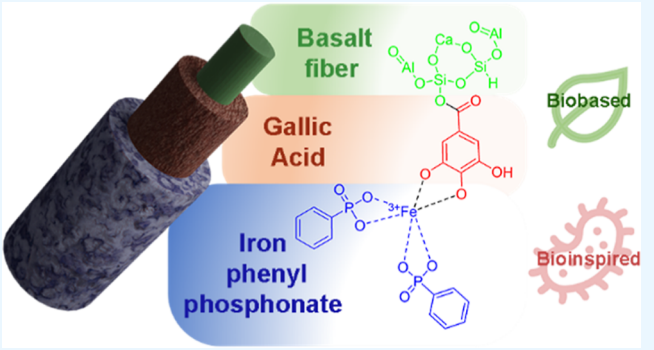

1. INTRODUCTION

In recent years, the growing awareness of environmental issues has led to various local, national, and even global regulations (such as the Kyoto Protocol), which aim to direct industries toward reducing their environmental impact and encouraging the use of renewable raw materials.[1,2]

In response to these regulations, industries and academic research have focused on the development of high-performance materials derived from natural sources.

In this context, biocomposite materials are attracting significant interest. Natural fiber-reinforced biopolymers[3] have been proposed as a sustainable alternative to traditional high-performance fiber-reinforced polymer (FRP) composites.[4]

One widely used biopolymer is poly(lactic acid) (PLA).[5] PLA has unique characteristics, such as high transparency and rigidity, making it the most investigated biodegradable aliphatic thermoplastic polyester as an alternative to conventional polymers.[6]

Many studies in the literature[7] have explored the reinforcement of PLA with plant fibers to obtain composites with good physical and mechanical properties. Examples include PLA reinforced with flax,[8] hemp,[9] bamboo,[10] and ramie[11] fibers. Due to their advantageous properties, low production costs, and environmentally sustainable profile, natural fiber-reinforced PLA composites find application in aerospace and automotive industries.[12] For instance, cotton fiber-reinforced PLA is used for noise reduction, and hemp, flax, and sisal are employed in the production of floor panels for automotive applications.[13] Despite their merits, these biocomposites are primarily suited for less-demanding nonstructural applications. For load-bearing parts requiring improved mechanical properties, synthetic-type fiber reinforcement is usually required.[14] Basalt fibers (BFs), obtained from basalt rock, have emerged as a promising reinforcement for FRPs amid growing environmental concerns. In fact, not only are BFs naturally occurring, but they also feature high specific stiffness, corrosion resistance, electrical insulation, and resistance to high temperatures.[15] These properties make BFs as an alternative to

Received: December 18, 2023
Revised: March 28, 2024
Accepted: April 9, 2024
Published: April 19, 2024

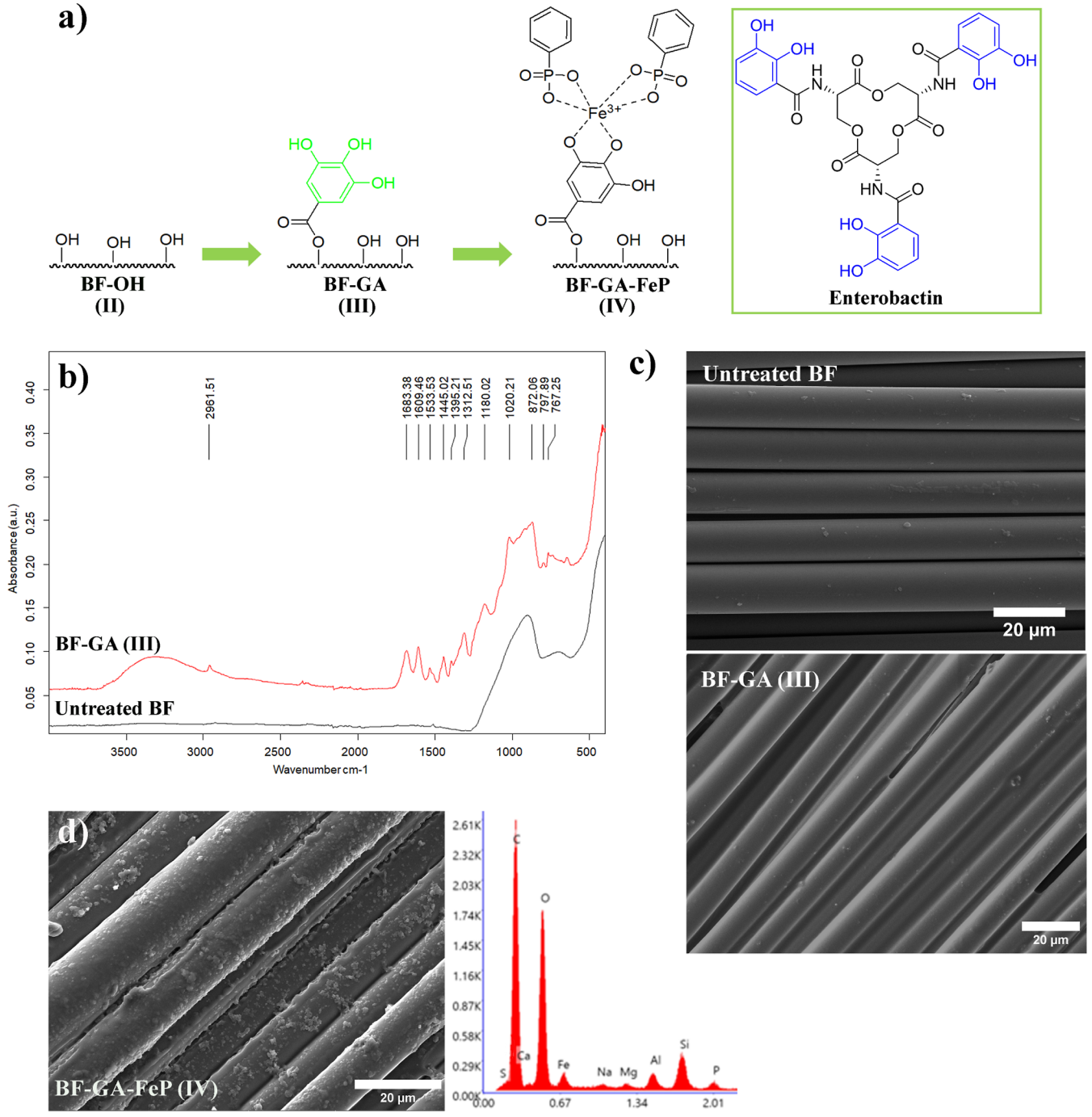

Figure 1. (a) Schematic representation of BF surface modification. (b) IR spectrum of the untreated BF (black line) and BF-GA, **III** (red line). (c) SEM micrographs of untreated BF and BF-GA, **III**. (d) SEM-EDS analysis of BF-GA-FeP (**IV**).

conventional synthetic fibers, showing, in particular, superior physical and mechanical properties compared to glass fibers, while being more sustainable and cost-effective than carbon fibers.[16] Basalt therefore emerges as a high-performance alternative to plant fibers and proves to be a more sustainable option than synthetic fibers.[17]

BF−PLA composites, given their good mechanical properties and biodegradability, find applications in the medical field, particularly in the production of medical devices and materials for bone repair.[18] Tábi et al. demonstrated that PLA reinforced with short BFs, processed using conventional twin-screw extrusion and injection molding techniques, could also be used in structural applications.[19] Current research is largely focused on improving the fiber−matrix interfacial adhesion due to the relatively chemically inert surface and low surface free energy of BFs.[20−22]

FRPs, particularly PLA composites, because of their polymer matrix, have an inherent tendency to burn quickly in case of fire.[23−25] Therefore, flame retardants (FRs) must be used to improve their flammability resistance and meet the industrial regulatory standards.[26] The incorporation of FRs directly into the polymer matrix is the most common method to improve the flammability resistance of FRPs. Incorporation of ammonium polyphosphate was found to be effective in flame

https://doi.org/10.1021/acsomega.3c10129
ACS Omega 2024, 9, 19099−19107

retardancy of PLA composites reinforced with kenaf[27] and ramie fibers.[28]

However, direct incorporation of FR into the matrix often reduces composite mechanical performance as the two components are often incompatible.[29] Yargici Kovanci et al. tested six different types of phosphorus-based FRs to increase the fire resistance of a glass-fiber-reinforced PLA (GF-PLA) composite. For the identification of the best FR, the six types were first tested on neat PLA samples, and it was observed that all of them had a negative effect on the final mechanical performance. The study identified a diphosphoric acid−based FR (P/N) coupled with a chain modifier as the optimal solution for GF-PLA composites. This chain modifier, in addition to optimizing the flame retardancy by reducing the candlewick effect, was effective in improving the mechanical performance of the composite.[30]

Another approach is to graft the FR directly onto the reinforcing fiber. This strategy reduces the "candlewick effect" and does not compromise the mechanical properties of the composite.[31] It is particularly used for composites reinforced with natural fibers, where the functional groups of these latter can be exploited to covalently link suitable FRs.[32]

BFs present a challenge due to their inert surface and limited polar groups, making the flame-retardant-fiber interaction difficult. Interestingly, Jiang et al.[33] and Liu et al.[34] reported that grafting organic-type FRs onto the glass fiber surface improves the fiber−matrix interfacial compatibility, resulting in a composite with enhanced flame resistance and mechanical properties.

The current legislative measures restricting the use of halogenated FRs[35] have stimulated the research area of phosphorus-based FRs, valued for their low toxicity and ability to act in both the condensed and gaseous phases when properly designed.[36]

In this work, we present a novel, bioinspired protocol for coating BFs with a halogen-free, phosphorus-based material from a renewable source designed for FR applications in biocomposite materials (Figure 1a). Specifically, a system incorporating iron phenyl phosphonate was developed. Literature reports indicate the efficacy of iron phosphonate as a FR in both condensed and gas phases.[37,38] It is expected that the developed coated fibers, when used as a reinforcement in composite materials, will generate phosphoric acid in the event of a fire, thus promoting the formation of a char layer and releasing low reactive radical species, inhibiting the combustion process. The coating also includes gallic acid (GA) units. GA is a biosourced phenolic acid that is present in vegetal biomass, both "as is" or as part of tannins.[39]

Once the commercial sizing was removed from the BF (**I**), for grafting the coating onto the surface, three steps were undertaken: (1) pretreatment of the chemically inert fiber with O_3,[40] which led to the formation of free −OH groups and resulted in BF−OH (**II**). The new functional groups were exploited for (2) covalent immobilization of GA units via ester bond formation,[41] yielding the modified fiber BF-GA (**III**); and (3) the in situ complexation of an iron phenyl phosphonate layer, obtaining the coated fiber denoted as BF-GA-FeP (**IV**) (Figure 1a).

This strategy was inspired by the bacterial bioprocess of acquiring iron from the surrounding environment. Bacteria secrete siderophores, small molecules that act as powerful chelating agents for iron intracellular transport.[42] Among their chelating functionalities, siderophores have catecholate groups. One of the most effective siderophores is enterobactin (Figure 1a), a triscatechol derivative of a cyclic triserine lactone. The catecholate groups are capable of strong coordination with a central ferric ion.[43] Leveraging the structural similarity with catechols, in this work, the GA units immobilized on the fiber surface were exploited for Fe^{III} coordination. Next, phenylphosphonic acid (PPA) was added to the system, resulting in the formation of the iron phenyl phosphonate complex.[44]

The modified BFs were characterized to confirm the effectiveness of the developed coating process by Fourier transform infrared spectroscopy (FT-IR), thermogravimetric analysis (TGA), scanning electron microscopy coupled with energy-dispersive X-ray spectroscopy (SEM-EDS), and microwave plasma atomic emission spectroscopy (MP-AES). Subsequently, these fibers were used as reinforcement in a PLA biocomposite, and the fire resistance of the biocomposite was evaluated.

To the best of the authors' knowledge, this method of coating BFs for improving fire resistance of polymer composites is a novel and previously unexplored approach.

2. RESULTS AND DISCUSSION

Considering the inherently inert nature of the BF surface, the sizing on the surface of the commercial BFs was removed by immersing them in acetone solvent at room temperature, avoiding the use of a commonly used Soxhlet extraction, which requires an operating temperature of 70 °C.[45] This procedure, which makes free −OH groups available again, provided results comparable to those obtained by refluxing the sample using acetone.[45] Furthermore, the use of acetone in this process allowed for nearly quantitative recovery through distillation from extracted sizing, enabling its reuse in subsequent treatments.

As shown in Figure S1a, the infrared (IR) spectra of sizing-free BF (**I**) and untreated BF show a broad absorption in the 800−1200 cm^{-1} range, ascribed to the antisymmetric stretching vibration of Si−O−Si in the BF.[45] In the IR spectrum of untreated BF, the absorptions at 1510 cm^{-1} can be assigned to the C−C stretching of aromatic rings, respectively, typical of epoxy resin sizing.[46] These signals disappear in the spectrum of **I**, confirming the acetone treatment's effectiveness.

To further validate the procedure, the sizing extracted was analyzed by FT-IR. The IR spectrum (Figure S1b) revealed the characteristic absorptions of epoxy resins: 1608 cm^{-1} (C═C stretching of aromatic rings), 1509 cm^{-1} (C−C stretching of the aromatic groups), 1039 cm^{-1} (ethers C−O−C stretching), and 828 cm^{-1} (C−O−C stretching of the oxirane group).[46]

The SEM micrographs of the untreated BF (Figure S2a) revealed the presence of sizing, whereas in the SEM micrographs of **I** (Figure S2b), the sizing was markedly reduced.

Following sizing removal, BFs were pretreated with ozone (O_3) to further increase their surface −OH groups (**II**).[40] O_3 was proposed as a safer alternative to other chemical agents such as the piranha solution, which is highly corrosive and difficult to handle.[47] Figure S3a shows the FT-IR spectra of **I** and **II**. The spectrum of **II** showed new absorptions at 1637 and 3365 cm^{-1} associated with adsorbed water and Si−OH stretching, respectively,[40] which confirm the formation of oxygen-containing functional groups on the BF surface. SEM analysis did not highlight any significant alteration in the fiber surface morphology (Figure S3b).

https://doi.org/10.1021/acsomega.3c10129
ACS Omega 2024, 9, 19099−19107

Untreated BF, **I**, and **II** were analyzed by TGA (Figure S4a,b). The approximate 0.82% reduction of the untreated BF in the temperature range 200−300 °C was attributed to the decomposition of commercial sizing. Sample **I** showed a lower weight reduction (0.41%) resulting from partial removal of commercial sizing by acetone treatment.[48] The thermogram of **II** exhibited a weight loss between 70 and 170 °C caused by the loss of physically adsorbed water molecules. The weight loss in the temperature range of 200−300 °C (0.72%) was higher than in the thermal decomposition of **I**, which is presumably due to the loss of surface hydroxyl groups.[49] The analyses revealed no significant weight reduction associated with the degradation of BFs up to 600 °C.

Subsequently, the pretreated fibers (**II**) underwent surface-modification with the newly designed coating. The first step involved the covalent immobilization of GA units on the fiber (**III**) by exploiting the reaction of its acyl chloride derivative[50] with the −OH groups at the fiber surface, leading to the formation of ester bonds (Figure 1a).[17]

The green solvent tert-amyl methyl ether (TAME)[51,52] was employed to this purpose (30% w/w).[41]

FT-IR analysis was used for the characterization of **III**, and Figure 1b presents a comparison of the spectrum of **I** and **III**. The **III** sample showed signals that can be associated with the GA units bound to the fiber: the broad absorption in the range between 3000 and 3600 cm^{-1} is due to the O−H stretching of the phenolic ring; the absorptions at 1611, 1525, and 1445 cm^{-1} are due to C−C stretching of the aromatic ring.[53] The signals at 1270 and 1017 cm^{-1}, together with the general absorption pattern observed in the 1000−1300 cm^{-1} range, are due to the C−O stretching and O−H bending,[54] respectively.

The surface morphology of **III** was characterized by SEM, as shown in Figure 1c. The typical smooth surface of the BF is replaced by a rough coating, and the gaps between the fibers are no longer visible.

The phenolic groups of the GA units were then exploited for the complexation of Fe^{III}.[43] The reaction took place in water at room temperature, taking advantage of the dissociation of $FeCl_3$ into $Fe(OH)_3$ and HCl in water. This process provided the necessary Fe(III) ions for complexation with the oxygen atoms of the phenolic groups, maintaining a pH < 5. Under these pH conditions,[55] mono(catecholate)iron(III) complexes can be obtained. PPA was then introduced into the reaction system. The oxygen atoms of the phosphonate moiety exhibit strong binding affinity to Fe^{III}, leading to the formation of iron phosphonate.[56] This compound was tightly bound to the fiber surface due to its complexation with GA units, resulting in the modified fiber denoted as **IV**.

Sample **IV** was further characterized by SEM-EDS analysis (Figure 1d), revealing a globular-shaped coating on the surface of the BF. The corresponding EDS spectrum confirmed the presence of P and Fe, providing evidence that the material bonded to the fiber was iron phosphonate resulting from the Fe^{III}—GA unit complexation.

The amount of Fe on **IV** was measured by MP-AES analysis using the untreated fiber as a blank sample. The sample showed an iron loading of 0.1 wt %, a low amount but nevertheless confirming the Fe^{III}—GA unit complexation on the BF surface.

TGA of the untreated fiber and **IV** (Figure S5a,b) revealed distinct weight loss patterns. Untreated BF showed an approximate 0.82% weight loss in the temperature range 200−300 °C, attributed to the degradation of commercial sizing. TGA performed on **IV** revealed two steps of weight loss in the temperature range of 170−270 and 270−400 °C with an approximate 1.83 wt % in the first range, attributed to the decomposition of GA units.[57−59] The approximate 5.41 wt % in the temperature range 270−400 °C of **IV** could be assigned to the breaking of C−C, C−H, and C−P bonds, which are all present in the structure of phenyl phosphonic units.[60,61]

To gain further insights into the formation of the phosphonate-iron-GA complex (GA-FeP), a reaction in homogeneous phase was performed, employing methyl gallate (MeGA) as a model substrate. MeGA underwent reaction in water with $FeCl_3$ to achieve complexation of Fe^{III} with phenolic groups, and, subsequently, PPA was added to enable the coordination of iron with the phosphonate, resulting in the formation of MeGa-FeP (see the Supporting Information).

MeGA and MeGa-FeP were characterized by UV−vis analysis (Figure S6). Pure MeGA exhibited a maximum absorbance at 280 nm.[62] The absorption spectrum of MeGa-FeP showed a shift in the position of λ_{max}, likely attributed to the presence of the phenyl phosphonic units absorbing in the same region,[63] while the complexation of Fe^{III} with the galloyl moiety resulted in absorption at higher wavelengths.[64]

The formation of the resulting homogeneous phosphonate-iron-GA complex was confirmed by nuclear magnetic resonance (NMR) (^{1}H NMR and ^{31}P NMR) analyses (Figures S7 and S8).

The fibers coated with the target complex (**IV**) were then used as a reinforcement for the manufacture of PLA-based composites.

Figure S9a,b shows the TG and DTG curves of pure PLA and PLA composites, while Table S1 shows the temperature values at 5 and 10% decomposition ($T_d^{5\%}$ and $T_d^{10\%}$), temperature at the maximum decomposition rate (T_d^{Max}), and residue obtained. The thermogram of neat PLA shows a one-stage complete degradation between about 300 and 400 °C. As for PLA, when reinforced with untreated BFs (PLA/BF), the thermal degradation process initiates at lower temperatures. Specifically, the temperature for 5% weight loss is 333.3 °C for PLA and 328.5 °C for PLA/BF. PLA is known to be extremely sensitive to the presence of moisture during the melt-processing as temperature and traces of water induce hydrolysis of ester bonds, leading to random-main chain scission.[65] During the microcompounding process, the polar nature of the BF likely retained residual moisture that induced hydrolysis and contributed to lower PLA degradation temperature.[66] The temperature values for 5% weight loss and other relevant temperatures (Table S1) were shifted to higher temperatures for treated fiber-reinforced PLA (PLA/BF-FeP), demonstrating the effectiveness of the developed coating complex in increasing the thermal stability of the composite. As-synthesized iron-phenyl-phosphonate was added to neat PLA with a concentration of 1 wt % (PLA-FeP) and characterized by TGA. The temperature at 5 and 10% decomposition and the temperature at the maximum decomposition rate (Table S1) turn out to be higher compared to that of pure PLA, as additional evidence of the effectiveness of the developed complex in enhancing the thermal stability of PLA. To evaluate the treated fiber char production efficiency, the residue weight of composites was assessed at 800 °C. However, due to the low complex loading on the fiber, as also detected by MP-AES analysis, no significant change in the residue amount was observed. Thus, even with a minimal

https://doi.org/10.1021/acsomega.3c10129
ACS Omega 2024, 9, 19099−19107

amount of the developed coating on the fiber surface, the composite showed increased thermal stability.

Pure PLA and composites were analyzed by differential scanning calorimetry (DSC) analysis. Table S2 shows the glass transition temperature (T_g), the peak temperature of the cold crystallization (T_{cc}) and melting (T_m) processes, the enthalpies involved in both transitions, and the calculated crystallinity degree (χ_c). To compare the thermal properties of composites and neat PLA, the data were determined on the second heating curve in order to delete the thermal history of all samples. Table S2 shows no significant variations among the parameters of PLA, PLA/BF, and PLA/BF-FeP; thus neither the 20% BF loading nor the developed coating affects the thermal properties of PLA. On the other hand, the T_{cc} of FeP-added PLA shifted to a lower temperature than that of the neat PLA sample, proving that the developed complex promotes the nucleation phase of the crystallization process. In fact, an increase in the χ_c of the FeP-added PLA compared with that of neat PLA is observed.[67] Given the low loading on the fiber surface, the developed complex does not affect the crystallinity of PLA in the PLA/BF-FeP composite.

Cone calorimeter tests are commonly used to assess the combustion behavior of materials under real fire condition.[68,69] Table S3 shows an overview of the key parameters evaluated for PLA/BF and PLA/BF-FeP, including time to ignition (TTI), time to flame out, peak of heat release rate (pHRR), total heat release, and total smoke production (TSP). Tests were carried out with a heat flow of 35 kW/m^2, which can be roughly compared to a medium scale fire. The TTI of PLA/BF-FeP composites exhibited a slight increase compared with uncoated fiber-reinforced PLA, while time to flame out is significantly reduced. Notably, the pHRR of PLA/BF-FeP experienced an 8% decrease compared to that of PLA/BF even at a very low loading of GA-FeP complex FR on BFs. These latest experimental evidence means that the fire propagating index (FPI = pHRR/TTI ratio) of PLA/BF-FeP (4.8 kW/m^2 s) is much lower than that of PLA/BF (5.6 kW/m^2 s). Thus, the GA-FeP complex-functionalized composite tends to be less prone to propagating the fire. TSP turns out to minimal for PLA/BF due to the reduced smoke generation of PLA during combustion,[44,70] and the BF does not contribute to this phenomenon. The PLA/BF-FeP composite showed no change in TSP. Studies are reported in the literature detecting an increase in TSP when phenyl phosphonate FRs are used due to the production of phosphorus free radicals acting in the gas phase.[71−73] The efficacy of the developed FR coating is noteworthy, given its low loading on the fiber surface, as it successfully mitigated smoke production without compromising its FR capabilities. Consistent with the TGA and MP-AES results, the low FR loading on the fibers does not lead to an appreciable decrease in the mass loss attributable to char production.

3. CONCLUSIONS

A sustainable and energy-saving bioinspired method for surface functionalization of BFs with iron phenyl phosphonate has been proposed and successfully implemented, offering a promising solution to the growing demand for sustainable products. The designed coating is not only bioderived but also employs green solvents such as TAME, while circumventing the need for high reaction temperatures.

Characterization of the modified fiber through SEM-EDS, FT-IR, TGA, and MP-AES analyses demonstrates the effectiveness of the treatment for the BF coating, which was further investigated by assessing its effects on PLA-based biocomposites.

Despite an extremely low FR loading on the fiber surface, the modified composites showed enhanced thermal stability, increased TTI, and reduced time to flame out, and simultaneously an 8% reduction in pHRR and a 15% reduction in FPI compared with the untreated BF reinforced composite. Remarkably, this minimal FR loading is adequate to improve the fire properties of the composites without contributing to increased TSP.

The confirmed efficacy of the treatment for coating BFs, characterized by an inert surface and reduced polar groups, suggests its potential applicability to different types of fibers, such as plant-based fibers, possessing surface functional groups able to bind the developed complex.

In conclusion, this work proposes an ecofriendly approach to address the poor fire resistance and low thermal stability of natural fiber composites, opening avenues for further advancements in sustainable materials.

4. MATERIALS AND METHODS

4.1. Materials. Chopped BFs, characterized by sizing compatible with epoxy resins, were provided by Basaltex. The nominal fiber length was 3.2 mm, with an average diameter of 13 μm. A PLA Luminy LX175 (96% L-isomer)) provided by TotalEnergies Corbion was used as the matrix material.

GA ($C_7H_6O_5$) was obtained from Thermo Scientific. Tetrahydrofuran (THF), thionyl chloride ($SOCl_2$), TAME, acetone (C_3H_6O), iron(III) chloride hexahydrate ($FeCl_3 \cdot 6H_2O$), phenylphosphonic acid (PPA, $C_6H_5P(O)(OH)_2$), and methanol (CH_3OH) were purchased from Merck KGaA, Darmstadt, Germany, and used without further purification unless otherwise noted.

4.2. Characterization Techniques. NMR spectroscopy was used to characterize the synthesis products. NMR spectra were recorded on a Bruker DRX-ADVANCE 400 MHz system (1H at 400 MHz and 13C at 100.6 MHz), using tetramethylsilane (TMS) as an internal standard. Deuterated chloroform ($CDCl_3$) and Dimethyl sulfoxide (DMSO-d_6) were used as solvents.

FT-IR spectroscopy was used to assess the efficacy of the sizing removal, O_3 pretreatment, and coating on the BF. IR spectra were recorded on a Bruker VERTEX 70 spectrometer, equipped with a diamond attenuated total reflectance (ATR) cell. FTIR-ATR spectra were acquired with a resolution of 4 cm^{-1}, in the mid-IR region (400−4000 cm^{-1}), collecting 128 scans.

The fiber surface morphology was studied by using a field emission scanning electron microscope coupled with energy-dispersive spectroscopy. Micrographs were acquired on a Tescan Mira3 system using a 10 kV acceleration voltage. The samples were earlier sputter coated with carbon.

A SDT-Q600 thermoanalyzer (TA Instruments) was used to determine the thermal properties of treated and untreated fibers and the manufactured composites. TGA was conducted in air or nitrogen from room temperature to 800 °C under a heating rate of 10 °C/min.

The glass transition, melting, and cold crystallization temperatures of all the samples were determined by means of (DSC 250 calorimeter, TA Instruments). The heating and cooling rate were set at 10 °C/min, and a high purity nitrogen with a flow rate of 40 mL/min was used. 10 mg of each sample

https://doi.org/10.1021/acsomega.3c10129
ACS Omega 2024, 9, 19099−19107

was first melted by heating up to 200 °C from 10 °C (5 min hold), and then they were crystallized by cooling to 10 °C (5 min hold). In order to remove the thermal history of the samples, the thermal program was repeated twice. Melting and cold crystallization enthalpies were determined, and the crystallinity degree of the samples was calculated according to eq 1

$$\chi_c = \frac{(\Delta H_m - \Delta H_{cc})}{\Delta H_m^0 x \varphi} \times 100 \quad (1)$$

where ΔH_m is the measured melting enthalpy of PLA composites, ΔH_{cc} is the measured cold crystallization enthalpy of PLA composites, φ is the polymer weight fraction in composites, and ΔH_m^0 = 93 J/g is the enthalpy of fusion of 100% crystalline PLA.[74]

Detection of the iron content in BF-GA-FeP was performed with an MP-AES 4210 instrument.

UV−vis absorption spectra of MeGa and MeGA-FeP complex were recorded with a UV-2700 Shimadzu Co. (Kyoto, Japan) spectrophotometer.

Fire behavior was assessed using an oxygen consumption cone calorimeter (Fire Testing Technology Limited FFT Cone Calorimeter model). The tests, following ISO 5660, were performed at an incident Heat flux of 35 kW/m^2 in horizontal orientation using the cone shaped heater and specimens of 100 × 100 mm^2 and thickness of 4 mm. Three samples were tested per each formulation.

4.3. Methods. *4.3.1. Sizing Removal from Basalt Fibers.* 150 g of BFs was placed in a reactor, and 1 L of acetone was added. The reactor was sealed, and the fibers were allowed to soak for 48 h at room temperature. The fibers were then washed with deionized H_2O, left to soak for 2 h, and dried in a ventilated oven at 80 °C. The extracted sizing was concentrated by solvent evaporation and analyzed by FT-IR spectroscopy. Before analysis, residual acetone was evaporated directly on the ATR crystal. The evaporated solvent was reused for further 3 representative treatments of BFs.

4.3.2. BF Ozonization Process. The fibers were pretreated with O_3. A Salinovo ozone generator was used, fed by air, and with a maximum diffusion rate of 0.5/h. 50 g of BF was placed in the ozone chamber, having a volume of 500 cm^3, and ozone was fluxed inside through a porous diffusion plate. The treatment was carried out for a maximum time of 7 h.

4.3.3. Synthesis of Galloyl Chloride. GA (63.75 g, 374 mmol) and anhydrous THF (45 mL, 701 mmol) were introduced in a dried single-necked flask. Thionyl chloride (90 mL, 461 mmol) and *N*,*N*-dimethylformamide (DMF) (0.35 mL, 4.5 mmol) were subsequently added. The reaction mixture was heated to 80 °C for 3 h. After the reaction time, the solvent and excess $SOCl_2$ has been removed under vacuum from the reaction mixture. The crude galloyl chloride was used for the subsequent reaction without further purification.

FT-IR (cm^{-1}): 2800−3400 (O−H stretching); 1715, 1632 (C═O stretching); 736, 693, 646, 589 (C−Cl stretching).[75]

^{1}H NMR (400 MHz, chloroform-*d*): δ 7.46 (s, 2H, Ar−H).

4.3.4. BF Coating. The crude galloyl chloride (92.34 g) was dissolved in TAME (215.4 g, 2.1 mol) to obtain a 30% w/w solution. 70 g of BF was immersed in the solution, and the system was kept under stirring for 2 h. The resulting sample was then washed with deionized H_2O and dried in a ventilated oven at 100 °C for 2 h.

The fibers functionalized by GA units (BF-GA) were transferred into a vessel containing 400 mL of deionized H_2O to which 100 mL of $FeCl_3{\cdot}6H_2O$ (3.15 g, 0.01 mol) aqueous solution was added. The system was kept under stirring, and PPA (3.69 g, 0.02 mol) dissolved in 100 mL of deionized H_2O was added dropwise after 6 h. The reaction proceeded at room temperature for 12 h. Iron phosphonate-modified BFs (FeP-BF) were washed with deionized water and dried overnight in a ventilated oven at 85 °C.

4.3.5. Composite Manufacturing. The manufacturing of PLA/BF, PLA/BF-FeP, and PLA/FeP composites was performed by traditional thermoplastic processes using a Brabender-like apparatus (Rheocord EC, Haake Inc.) to prepare compounds and transforming the same in plates of suitable sizes with the aid of a lab hydraulic press (Collin model P400E). Before compounding, the chopped BF, BF-GA-FeP, and as-synthesized iron-phenyl-phosphonate as well as the PLA pellets were dried in a vacuum oven at 70 °C for 4 h. The micro compounder was used to mix BF, BF-GA-FeP, and iron-phenyl-phosphonate with PLA setting the rotation speed of 60 rpm at 180 °C for 5 min. The PLA composites were then compression-molded at 180 °C using a pressure profile selected essentially on the basis of previous experiences (2 min at 0 bar −1 min at 5 bar −1 min at 10 bar and 1 min at 20 bar). Finally, the cooling step to room temperature was carried out while maintaining the material at the maximum pressure set (20 bar). The fiber content was kept at 20 wt %.

4.3.6. MP-AES Analysis. 15 mg of the sample (FeP-BF and fibers as blank) was digested in a 20 mL graduated flask using 4 mL of aqua regia mixture (3:1 HCl/HNO_3). After 3 h, deionized water was used to reach the final volume, and the residual solid fibers were filtered. The solutions were analyzed by using a MP-AES 4210 instrument.

■ ASSOCIATED CONTENT

Supporting Information

The Supporting Information is available free of charge at https://pubs.acs.org/doi/10.1021/acsomega.3c10129.

MeGA-FeP complex synthesis protocol; infrared spectra of untreated BF, **I** (sizing-free BF), and extracted sizing; SEM micrographs of untreated BF and **I** (sizing-free BF); infrared spectrum of **I** (BF−OH); SEM micrograph of **II** (BF−OH); TGA and DTG curves of untreated BF, **I** (sizing-free BF), **II** (BF−OH), and **IV** (BF-GA-FeP); UV−vis absorption spectra of MeGA and MeGa-FeP; ^{1}H NMR and ^{31}P NMR spectra of the MeGA-FeP complex; TG and DTG curves of neat PLA and composites and their corresponding temperatures at 5% ($T_d^{5\%}$) and 10% ($T_d^{10\%}$) weight loss, at maximum decomposition rate (T_d^{Max}), and residue weight at 800 °C (Residue); thermal behavior of PLA and composites measured by DSC experiments; and cone calorimetry data of PLA/BF and PLA/BF-FeP composites (PDF)

■ AUTHOR INFORMATION

Corresponding Author

Alessia Pantaleoni − *Department of Chemical Engineering Materials Environment, Sapienza University of Rome, Rome 00184, Italy;* orcid.org/0009-0008-1207-6500; Email: alessia.pantaleoni@uniroma1.it

https://doi.org/10.1021/acsomega.3c10129
ACS Omega 2024, 9, 19099−19107

Authors

Fabrizio Sarasini − *Department of Chemical Engineering Materials Environment, Sapienza University of Rome, Rome 00184, Italy;* orcid.org/0000-0001-5233-8589

Pietro Russo − *Institute for Polymers, Composites and Biomaterials, National Research Council, Pozzuoli, NA 80078, Italy*

Jessica Passaro − *Institute for Polymers, Composites and Biomaterials, National Research Council, Pozzuoli, NA 80078, Italy;* orcid.org/0000-0002-6588-2580

Loris Giorgini − *Department of Industrial Chemistry "Toso Montanari", University of Bologna, Bologna 40136, Italy;* orcid.org/0000-0003-2248-3552

Irene Bavasso − *Department of Chemical Engineering Materials Environment, Sapienza University of Rome, Rome 00184, Italy*

Maria Laura Santarelli − *Department of Chemical Engineering Materials Environment, Sapienza University of Rome, Rome 00184, Italy*

Elisabetta Petrucci − *Department of Chemical Engineering Materials Environment, Sapienza University of Rome, Rome 00184, Italy;* orcid.org/0000-0003-4282-4780

Federica Valentini − *Department of Chemistry, Biology and Biotechnology, University of Perugia, Perugia 06123, Italy*

Maria Paola Bracciale − *Department of Chemical Engineering Materials Environment, Sapienza University of Rome, Rome 00184, Italy;* orcid.org/0000-0002-3863-1188

Assunta Marrocchi − *Department of Chemistry, Biology and Biotechnology, University of Perugia, Perugia 06123, Italy*

Complete contact information is available at: https://pubs.acs.org/10.1021/acsomega.3c10129

Notes

The authors declare no competing financial interest.

■ ACKNOWLEDGMENTS

Financed by the European Union—NextGenerationEU (National Sustainable Mobility Center CN00000023, Italian Ministry of University and Research Decree n. 1033—17/06/2022, Spoke 11—Innovative Materials & Lightweighting). A.M. thanks the "**FASTTO0**" project (CUP J93C22000330006), funded through the Italian Ministry of Environment and Energy Security.

■ REFERENCES

(1) Hejna, A. Renewable, Degradable, and Recyclable Polymer Composites. *Polymers* **2023**, *15* (7), 1769.

(2) Bohringer, C. The Kyoto Protocol: A Review and Perspectives. *Oxford Rev. Econ. Policy* **2003**, *19* (3), 451−466.

(3) Madyaratri, E.; Ridho, M.; Aristri, M.; Lubis, R.; Iswanto, A.; Nawawi, D.; Antov, P.; Kristak, L.; Majlingová, A.; Fatriasari, W. Recent Advances in the Development of Fire-Resistant Biocomposites—A Review. *Polymers* **2022**, *14*, 362.

(4) Rajak, D.; Pagar, D.; Menezes, P.; Linul, E. Fiber-Reinforced Polymer Composites: Manufacturing, Properties, and Applications. *Polymers* **2019**, *11*, 1667.

(5) Aaliya, B.; Sunooj, K. V.; Lackner, M. Biopolymer Composites: A Review. *Int. J. Biobased Plast.* **2021**, *3* (1), 40−84.

(6) Getme, A. S.; Patel, B. A Review: Bio-Fiber's as Reinforcement in Composites of Polylactic Acid (PLA). *Mater. Today: Proc.* **2020**, *26*, 2116−2122.

(7) Azlin, M. N. M.; Sapuan, S. M.; Zainudin, E. S.; Zuhri, M. Y. M.; Ilyas, R. A. *Natural Polylactic Acid-Based Fiber Composites: A Review*; Elsevier Inc., 2020.

(8) Georgiopoulos, P.; Christopoulos, A.; Koutsoumpis, S.; Kontou, E. The Effect of Surface Treatment on the Performance of Flax/Biodegradable Composites. *Composites, Part B* **2016**, *106*, 88−98.

(9) Sawpan, M. A.; Pickering, K. L.; Fernyhough, A. Improvement of Mechanical Performance of Industrial Hemp Fibre Reinforced Polylactide Biocomposites. *Composites, Part A* **2011**, *42* (3), 310−319.

(10) Kang, J. T.; Kim, S. H. Improvement in the Mechanical Properties of Polylactide and Bamboo Fiber Biocomposites by Fiber Surface Modification. *Macromol. Res.* **2011**, *19* (8), 789−796.

(11) Yu, T.; Ren, J.; Li, S.; Yuan, H.; Li, Y. Effect of Fiber Surface-Treatments on the Properties of Poly(Lactic Acid)/Ramie Composites. *Composites, Part A* **2010**, *41* (4), 499−505.

(12) Ilyas, R. A.; Sapuan, S. M.; Harussani, M. M.; Hakimi, M. Y. A. Y.; Haziq, M. Z. M.; Atikah, M. S. N.; et al. Polylactic Acid (PLA) Biocomposite: Processing, Additive Manufacturing and Advanced Applications. *Polymers* **2021**, *13*, 1326.

(13) Holbery, J.; Houston, D. Natural-Fiber-Reinforced Polymer Composites in Automotive Applications. *JOM* **2006**, *58* (11), 80−86.

(14) Sun, Y.; Zheng, Z.; Wang, Y.; Yang, B.; Wang, J.; Mu, W. PLA Composites Reinforced with Rice Residues or Glass Fiber—a Review of Mechanical Properties, Thermal Properties, and Biodegradation Properties. *J. Polym. Res.* **2022**, *29* (10), 422.

(15) Yang, G.; Park, M.; Park, S. J. Recent Progresses of Fabrication and Characterization of Fibers-Reinforced Composites: A Review. *Compos. Commun.* **2019**, *14*, 34−42.

(16) Li, Z.; Ma, J.; Ma, H.; Xu, X. Properties and Applications of Basalt Fiber and Its Composites. *IOP Conf. Ser.: Earth Environ. Sci.* **2018**, *186*, 012052.

(17) Jain, N.; Singh, V. K.; Chauhan, S. Review on Effect of Chemical, Thermal, Additive Treatment on Mechanical Properties of Basalt Fiber and Their Composites. *J. Mech. Behav. Mater.* **2017**, *26* (5−6), 205−211.

(18) Chen, X.; Li, Y.; Gu, N. A Novel Basalt Fiber-Reinforced Polylactic Acid Composite for Hard Tissue Repair. *Biomed. Mater.* **2010**, *5* (4), 044104.

(19) Tábi, T.; Bakonyi, P.; Hajba, S.; Herrera-Franco, P. J.; Czigány, T.; Kovács, J. Creep Behaviour of Injection-Moulded Basalt Fibre Reinforced Poly(Lactic Acid) Composites. *J. Reinf. Plast. Compos.* **2016**, *35* (21), 1600−1610.

(20) Ying, Z.; Wu, D.; Zhang, M.; Qiu, Y. Polylactide/Basalt Fiber Composites with Tailorable Mechanical Properties: Effect of Surface Treatment of Fibers and Annealing. *Compos. Struct.* **2017**, *176*, 1020−1027.

(21) Khandelwal, S.; Rhee, K. Y. Recent Advances in Basalt-Fiber-Reinforced Composites: Tailoring the Fiber-Matrix Interface. *Composites, Part B* **2020**, *192*, 108011.

(22) Kurniawan, D.; Kim, B. S.; Lee, H. Y.; Lim, J. Y. Atmospheric Pressure Glow Discharge Plasma Polymerization for Surface Treatment on Sized Basalt Fiber/Polylactic Acid Composites. *Composites, Part B* **2012**, *43* (3), 1010−1014.

(23) Kim, Y.; Lee, S.; Yoon, H. Fire-Safe Polymer Composites: Flame-Retardant Effect of Nanofillers. *Polymers* **2021**, *13* (4), 540.

(24) Tawiah, B.; Yu, B.; Fei, B. Advances in Flame Retardant Poly(Lactic Acid). *Polymers* **2018**, *10* (8), 876.

(25) Yiga, V. A.; Lubwama, M.; Pagel, S.; Benz, J.; Olupot, P. W.; Bonten, C. Flame Retardancy and Thermal Stability of Agricultural Residue Fiber-Reinforced Polylactic Acid: A Review. *Polym. Compos.* **2021**, *42* (1), 15−44.

(26) Kandola, B. K.; Kandare, E. Composites Having Improved Fire Resistance. In *Advances in Fire Retardant Materials*; Woodhead Publishing, 2008; pp 398−442..

(27) Shukor, F.; Hassan, A.; Saiful Islam, M.; Mokhtar, M.; Hasan, M. Effect of Ammonium Polyphosphate on Flame Retardancy, Thermal Stability and Mechanical Properties of Alkali Treated Kenaf Fiber Filled PLA Biocomposites. *Mater. Des.* **2014**, *54*, 425−429.

(28) Shumao, L.; Jie, R.; Hua, Y.; Tao, Y.; Weizhong, Y. Influence of Ammonium Polyphosphate on the Flame Retardancy Andmechanical

Properties of Ramie Fiber-Reinforced Poly(Lactic Acid) Biocomposites. *Polym. Int.* **2010**, *59* (2), 242−248.
(29) Guo, Y.; Zhou, M.; Yin, G.-Z.; Kalali, E.; Wang, N.; Wang, D.-Y. Basalt Fiber-Based Flame Retardant Epoxy Composites: Preparation, Thermal Properties, and Flame Retardancy. *Materials* **2021**, *14* (4), 902.
(30) Yargici Kovanci, C.; Nofar, M.; Ghanbari, A. Synergistic Enhancement of Flame Retardancy Behavior of Glass-Fiber Reinforced Polylactide Composites through Using Phosphorus-Based Flame Retardants and Chain Modifiers. *Polymers* **2022**, *14* (23), 5324.
(31) Shi, X.-H.; Li, X.-L.; Li, Y.-M.; Li, Z.; Wang, D.-Y. Flame-Retardant Strategy and Mechanism of Fiber Reinforced Polymeric Composite: A Review. *Composites, Part B* **2022**, *233*, 109663.
(32) Ferreira, D. P.; Cruz, J.; Fangueiro, R. Surface Modification of Natural Fibers in Polymer Composites. In *Green Composites for Automotive Applications*; Woodhead Publishing, 2019; pp 3−41..
(33) Jiang, J.; Cheng, Y.; Liu, Y.; Wang, Q.; He, Y.; Wang, B. Intergrowth Charring for Flame-Retardant Glass Fabric-Reinforced Epoxy Resin Composites. *J. Mater. Chem. A* **2015**, *3* (8), 4284−4290.
(34) Liu, L.; Liu, Y.; Han, Y.; Liu, Y.; Wang, Q. Interfacial Charring Method to Overcome the Wicking Action in Glass Fiber-Reinforced Polypropylene Composite. *Compos. Sci. Technol.* **2015**, *121*, 9−15.
(35) Hull, T. R.; Law, R. J.; Bergman, Å. Environmental Drivers for Replacement of Halogenated Flame Retardants. In *Polymer Green Flame Retardants*; Elsevier, 2014; pp 119−179..
(36) Morgan, A. B.; Wilkie, C. A. *Non-Halogenated Flame Retardant Handbook*; Wiley, 2014..
(37) Shi, X.-H.; Liu, Q.-Y.; Li, X.-L.; Yang, S.-Y.; Wang, D.-Y. Simultaneously Improving the Fire Safety and Mechanical Properties of Epoxy Resin with Iron Phosphonated Grafted Polyethylenimine. *Polym. Degrad. Stab.* **2022**, *206*, 110173.
(38) Yun, G. W.; Lee, J. H.; Kim, S. H. Flame Retardant and Mechanical Properties of Expandable Graphite/Polyurethane Foam Composites Containing Iron Phosphonate Dopamine-Coated Cellulose. *Polym. Compos.* **2020**, *41* (7), 2816−2828.
(39) Karamać, M.; Kosińska, A.; Pegg, R. B. Content of Gallic Acid in Selected Plant Extracts. *Pol. J. Food Nutr. Sci.* **2006**, *56* (1), 55−58.
(40) Kim, S.-H.; Park, S.-M.; Park, S.-J. Role of Dry Ozonization of Basalt Fibers on Interfacial Properties and Fracture Toughness of Epoxy Matrix Composites. *Nanotechnol. Rev.* **2021**, *10* (1), 710−718.
(41) Kanat, M.; Eren, T. Synthesis of Phosphorus-Containing Flame Retardants and Investigation of Their Flame Retardant Behavior in Textile Applications. *J. Appl. Polym. Sci.* **2019**, *136* (36), 47935.
(42) Raymond, K. N.; Allred, B. E.; Sia, A. K. Coordination Chemistry of Microbial Iron Transport. *Acc. Chem. Res.* **2015**, *48*, 2496−2505.
(43) Raymond, K. N.; Dertz, E. A.; Kim, S. S. Enterobactin: An Archetype for Microbial Iron Transport. *Proc. Natl. Acad. Sci. U.S.A.* **2003**, *100* (7), 3584−3588.
(44) Zhang, L.; Li, Z.; Pan, Y. T.; Yáñez, A. P.; Hu, S.; Zhang, X. Q.; Wang, R.; Wang, D. Y. Polydopamine Induced Natural Fiber Surface Functionalization: A Way towards Flame Retardancy of Flax/Poly(Lactic Acid) Biocomposites. *Composites, Part B* **2018**, *154*, 56−63.
(45) Xing, D.; Xi, X.-Y.; Ma, P.-C. Factors Governing the Tensile Strength of Basalt Fibre. *Composites, Part A* **2019**, *119*, 127−133.
(46) González, M. G.; Cabanelas, J. C.; Baselga, J. Applications of FTIR on Epoxy Resins—Identification, Monitoring the Curing Process, Phase Separation and Water Uptake. In *Infrared Spectroscopy—Materials Science, Engineering and Technology*; InTech, 2012.
(47) Zhang, X.; Zhou, X.; Ni, H.; Rong, X.; Zhang, Q.; Xiao, X.; Huan, H.; Liu, J. F.; Wu, Z. Surface Modification of Basalt Fiber with Organic/Inorganic Composites for Biofilm Carrier Used in Wastewater Treatment. *ACS Sustainable Chem. Eng.* **2018**, *6* (2), 2596−2602.
(48) Bhat, T.; Fortomaris, D.; Kandare, E.; Mouritz, A. P. Properties of Thermally Recycled Basalt Fibres and Basalt Fibre Composites. *J. Mater. Sci.* **2018**, *53*, 1933−1944.
(49) Zhang, L.; Kiny, V. U.; Peng, H.; Zhu, J.; Lobo, R. F. M.; Margrave, J. L.; Khabashesku, V. N. Sidewall Functionalization of Single-Walled Carbon Nanotubes with Hydroxyl Group-Terminated Moieties. *Chem. Mater.* **2004**, *16*, 2055−2061.
(50) Howell, B. A.; Oberdorfer, K. L.; Ostrander, E. A. Phosphorus Flame Retardants for Polymeric Materials from Gallic Acid and Other Naturally Occurring Multihydroxybenzoic Acids. *Int. J. Polym. Sci.* **2018**, *2018*, 1−12.
(51) Prat, D.; Wells, A.; Hayler, J.; Sneddon, H.; Mcelroy, C. R.; Abou-Shehada, S.; Dunn, P. J. CHEM21 Selection Guide of Classical- and Less Classical-Solvents. *Green Chem.* **2016**, *18*, 288−296.
(52) Ho, D.; Lee, J.; Park, S.; Park, Y.; Cho, K.; Campana, F.; Lanari, D.; Facchetti, A.; Seo, S. Y.; Kim, C.; Marrocchi, A.; Vaccaro, L. Green Solvents for Organic Thin-Film Transistor Processing. *J. Mater. Chem. C* **2020**, *8* (17), 5786−5794.
(53) Mohammed-Ziegler, I.; Billes, F. Vibrational Spectroscopic Calculations on Pyrogallol and Gallic Acid. *J. Mol. Struct. THEOCHEM* **2002**, *618* (3), 259−265.
(54) Naz, S.; Khaskheli, A. R.; Aljabour, A.; Kara, H.; Talpur, F. N.; Sherazi, S. T. H.; Khaskheli, A. A.; Jawaid, S. Synthesis of Highly Stable Cobalt Nanomaterial Using Gallic Acid and Its Application in Catalysis. *Adv. Chem.* **2014**, *2014*, 1−6.
(55) Sánchez, P.; Gálvez, N.; Colacio, E.; Miñones, E.; Domínguez-Vera, J. M. Catechol Releases Iron(III) from Ferritin by Direct Chelation without Iron(II) Production. *Dalton Trans.* **2005**, *4*, 811−813.
(56) Barja, B. C.; Herszage, J.; Dos Santos Afonso, M. Iron(III)-Phosphonate Complexes. *Polyhedron* **2001**, *20* (15−16), 1821−1830.
(57) Aytac, Z.; Kusku, S. I.; Durgun, E.; Uyar, T. Encapsulation of Gallic Acid/Cyclodextrin Inclusion Complex in Electrospun Polylactic Acid Nanofibers: Release Behavior and Antioxidant Activity of Gallic Acid. *Mater. Sci. Eng., C* **2016**, *63*, 231−239.
(58) Aydogdu, A.; Sumnu, G.; Sahin, S. Fabrication of Gallic Acid Loaded Hydroxypropyl Methylcellulose Nanofibers by Electrospinning Technique as Active Packaging Material. *Carbohydr. Polym.* **2019**, *208*, 241−250.
(59) Neo, Y. P.; Ray, S.; Jin, J.; Gizdavic-Nikolaidis, M.; Nieuwoudt, M. K.; Liu, D.; Quek, S. Y. Encapsulation of Food Grade Antioxidant in Natural Biopolymer by Electrospinning Technique: A Physicochemical Study Based on Zein-Gallic Acid System. *Food Chem.* **2013**, *136* (2), 1013−1021.
(60) Chakraborty, D.; Dam, T.; Modak, A.; Pant, K. K.; Chandra, B. K.; Majee, A.; Ghosh, A.; Bhaumik, A. A Novel Crystalline Nanoporous Iron Phosphonate Based Metal-Organic Framework as an Efficient Anode Material for Lithium Ion Batteries. *New J. Chem.* **2021**, *45*, 15458−15468.
(61) Bhanja, P.; Ghosh, K.; Islam, S. S.; Patra, A. K.; Islam, S. M.; Bhaumik, A. New Hybrid Iron Phosphonate Material as an Efficient Catalyst for the Synthesis of Adipic Acid in Air and Water. *ACS Sustainable Chem. Eng.* **2016**, *4*, 7147−7157.
(62) Zhang, L.; Liu, Y.; Wang, Y. Deprotonation Mechanism of Methyl Gallate: UV Spectroscopic and Computational Studies. *Int. J. Mol. Sci.* **2018**, *19*, 3111.
(63) Rajendran, S.; Apparao, B. V.; Palaniswamy, N. Mechanism of Inhibition of Corrosion of Mild Steel by Polyacrylamide, Phenyl Phosphonate and Zn2+. *Anti-Corros. Methods Mater.* **1999**, *46* (2), 111−116.
(64) Hynes, M. J.; Ó Coinceanainn, M. The Kinetics and Mechanisms of the Reaction of Iron(III) with Gallic Acid, Gallic Acid Methyl Ester and Catechin. *J. Inorg. Biochem.* **2001**, *85* (2−3), 131−142.
(65) Porfyris, A.; Vasilakos, S.; Zotiadis, C.; Papaspyrides, C.; Moser, K.; Van der Schueren, L.; Buyle, G.; Pavlidou, S.; Vouyiouka, S. Accelerated Ageing and Hydrolytic Stabilization of Poly(Lactic Acid) (PLA) under Humidity and Temperature Conditioning. *Polym. Test.* **2018**, *68*, 315−332.
(66) Sbardella, F.; Martinelli, A.; Di Lisio, V.; Bavasso, I.; Russo, P.; Tirillò, J.; Sarasini, F. Surface Modification of Basalt Fibres with Zno

https://doi.org/10.1021/acsomega.3c10129
ACS Omega 2024, 9, 19099−19107

Nanorods and Its Effect on Thermal and Mechanical Properties of Pla-Based Composites. *Biomolecules* **2021**, *11* (2), 200.
(67) Pan, H.; Kong, J.; Chen, Y.; Zhang, H.; Dong, L. Improved Heat Resistance Properties of Poly(L-Lactide)/Basalt Fiber Biocomposites with High Crystallinity under Forming Hybrid-Crystalline Morphology. *Int. J. Biol. Macromol.* **2019**, *122*, 848−856.
(68) Schartel, B.; Wilkie, C. A.; Camino, G. Recommendations on the Scientific Approach to Polymer Flame Retardancy: Part 1—Scientific Terms and Methods. *J. Fire Sci.* **2016**, *34* (6), 447−467.
(69) Schartel, B.; Wilkie, C. A.; Camino, G. Recommendations on the Scientific Approach to Polymer Flame Retardancy: Part 2—Concepts. *J. Fire Sci.* **2017**, *35* (1), 3−20.
(70) Qin, W.; Zhang, R.; Fu, Y.; Chang, J. Preparation of a Novel Bio-Based Ferric Flame Retardant for Enhancing Flame Retardancy, Mechanical Properties, and Heat Resistance of Polylactic Acid. *J. Appl. Polym. Sci.* **2023**, *140* (42), No. e54542.
(71) Liu, L.; Yan, C.; Zhang, W.; Xu, Y.; Xu, M.; Hong, Y.; Qiu, Y.; Li, B. A Monomolecular Organophosphate for Enhancing the Flame Retardancy, Thermostability and Crystallization Properties of Polylactic Acid. *J. Appl. Polym. Sci.* **2023**, *140* (4), No. e53347.
(72) Ma, X.; Wu, N.; Liu, P.; Cui, H. Fabrication of Highly Efficient Phenylphosphorylated Chitosan Bio-Based Flame Retardants for Flammable PLA Biomaterial. *Carbohydr. Polym.* **2022**, *287*, 119317.
(73) Jin, Q.; Tian, G. Q.; He, R.; Gu, H. L.; Wu, F.; Zhu, J. Simultaneously Enhancing the Crystallization Rate and Fire Retardancy of Poly(Lactic Acid) by Using a Novel Bifunctional Additive Trimethylamine Phenylphosphonate. *RSC Adv.* **2021**, *11* (44), 27346−27355.
(74) Turner, J. F.; Riga, A.; O'Connor, A.; Zhang, J.; Collis, J. Characterization of Drawn and Undrawn Poly-L-Lactide Films by Differential Scanning Calorimetry. *J. Therm. Anal. Calorim.* **2004**, *75* (1), 257−268.
(75) Mondal, K.; Sharma, S.; Kakkar, S.; Khatkar, A. Synthesis, Urease Inhibition, Antimicrobial and Antioxidant Studies of 3,4,5-Trihydroxy Benzoic Acid Derivatives. *Indo Global J. Pharm. Sci.* **2018**, *08* (01), 12−20.

https://doi.org/10.1021/acsomega.3c10129
ACS Omega 2024, 9, 19099−19107